

Real space topological invariant and higher-order topological Anderson insulator in two-dimensional non-Hermitian systems

Hongfang Liu,¹ Ji-Kun Zhou,¹ Bing-Lan Wu,¹ Zhi-Qiang Zhang,^{1,*} and Hua Jiang^{1,2,†}

¹*School of Physical Science and Technology, Soochow University, Suzhou, 215006, China*

²*Institute for Advanced Study, Soochow University, Suzhou 215006, China*

(Dated: February 25, 2021)

We study the characterization and realization of higher-order topological Anderson insulator (HOTAI) in non-Hermitian systems, where the non-Hermitian mechanism ensures extra symmetries as well as gain and loss disorder. We illuminate that the quadrupole moment Q_{xy} can be used as the real space topological invariant of non-Hermitian higher-order topological insulator (HOTI). Based on the biorthogonal bases and non-Hermitian symmetries, we prove that Q_{xy} can be quantized to 0 or 0.5. Considering the disorder effect, we find the disorder-induced phase transition from normal insulator to non-Hermitian HOTAI. Furthermore, we elucidate that the real space topological invariant Q_{xy} is also applicable for systems with the non-Hermitian skin effect. Our work enlightens the study of the combination of disorder and non-Hermitian HOTI.

PACS numbers:

I. INTRODUCTION

With the development of topological theory of Hermitian systems, many kinds of topological states have been proposed and realized^{1–14}, among which the non-Hermitian counterparts^{15–27} have attracted great attention. Compared with the Hermitian cases, the non-Hermitian topological states are based on the non-Bloch theory^{20–23} due to the unique features of non-Hermitian Hamiltonian^{19–24,29–32}. Soon after the establish of the non-Hermitian topological band theory, there is a blooming investigations of disorder effect^{32–42} in non-Hermitian systems. By using the non-commutative geometry method^{37–40,43–47}, the disorder-induced phase transitions of non-Hermitian Chern insulator^{37,38} and non-Hermitian Su-Schrieffer-Heeger model^{39,40} have been studied. The non-Hermitian topological Anderson insulator^{37–40} is also reported.

In these years, the Hermitian higher-order topological insulator (HOTI)^{48–60} is one of the most focus of topological states. Not only the nested-Wilson-loop method^{49–51} but also the real-space topological invariant^{56–60} were reported to characterize such states. Specially, in two-dimensional systems, the quadrupole moment Q_{xy} ^{56–60} was proposed to be the real space topological invariant of HOTI. Initially, the quantization of this topological invariant was thought to be protected by the point group in the HOTI⁵¹ which is considered as the topological crystal insulators¹³. However, Li *et al.*⁵⁸ showed that the quantized Q_{xy} could also be protected by chiral symmetry or particle-hole symmetry in Hermitian systems. Such results still hold even with disorder effects. They also carefully studied the disorder-induced phase transition in the corresponding systems and predicted the existence of a higher-order topological Anderson insulator (HOTAI).

Very recently, the interplay of HOTI and non-Hermitian is proposed and gains extensive interests^{24,25,62,63}. The topological invariants in momentum space to distinguish such topological phases are

also investigated^{24,25}. However, the researches referred to real space topological invariant and disorder-induced topological phase transition of non-Hermitian HOTI are seldom reported. Since the Hamiltonian $H \neq H^\dagger$, the chiral symmetry or particle-hole symmetry in Hermitian cases will change into the distinctive symmetries²⁷ in non-Hermitian cases. Moreover, disorders with gain and loss are also available for non-Hermitian samples. These features should affect the disorder effect and the related phase transitions, which is unique for non-Hermitian systems.

In this paper, we propose that the quadrupole moment Q_{xy} , defined in the frame of the biorthogonal bases^{20,21,38,64}, can be considered as the real space topological invariant of non-Hermitian HOTI. We prove that Q_{xy} is quantized to 0 or 0.5 if there is a real diagonal matrix connecting Hamiltonian H with $-H^\dagger$, which is universal for non-Hermitian samples with line gap along the real axis. Specifically, taking the pseudoanti-Hermiticity symmetry²⁴ as an example, we demonstrate that the quantized $Q_{xy} = 0.5$ can be utilized to identify the non-Hermitian HOTI. In terms of Q_{xy} , the disorder-induced topological phase transition in non-Hermitian HOTI is also studied. With the help of the pseudoanti-Hermiticity protected quantization of Q_{xy} , we uncover that the non-Hermitian HOTI is robust against disorder. More importantly, the non-Hermitian HOTAI is predicted in such a system. Finally, we manifest that Q_{xy} is also applicable for systems with non-Hermitian skin effect (NHSE)^{19,21,28–32}.

This paper is organized as follows: In Sec. II, we present the method and the model. We demonstrate the realization of non-Hermitian HOTAI in Sec. III. Then, a brief discussion and summary are presented in Sec. IV.

II. METHOD AND MODEL

A. Quantized quadrupole moment protected by pseudoanti-Hermiticity symmetry

We suppose a non-Hermitian Hamiltonian H holds the pseudoanti-Hermiticity symmetry η with $\eta = \eta^{-1}$ and $\eta H \eta = -H^\dagger$. Such symmetry extends the chiral symmetry in Hermitian cases²⁷. According to the properties of Hamiltonian in non-Hermitian systems, the eigenvalues of H and H^\dagger are given as follows⁶⁴:

$$H|\psi_r^n\rangle = E_n|\psi_r^n\rangle, \quad H^\dagger|\psi_l^n\rangle = E_n^*|\psi_l^n\rangle, \quad (1)$$

where $|\psi_r^n\rangle$ and $|\psi_l^n\rangle$ are the n th standard right and left eigenvectors, respectively. The spectrum of eigenvalues can be separated into two parts with $Re[E] > 0$ and $Re[E] < 0$, which implies a line gap along $Re[E]$. $Re[E]$ represents the real part of the eigenvalue E . We suppose all the occupied states with $Re[E] < 0$ ($Re[E^*] < 0$) construct a matrix U_r (U_l). On the other hand, the matrix V_r (V_l) constructed by the unoccupied states are shown in Fig. 1. Following the previous studies in Hermitian systems^{56–60}, we define the quadrupole moment in non-Hermitian systems as⁶¹:

$$Q_{xy} = \frac{1}{2\pi} \text{Im}\{\log[\det(U_l^\dagger \hat{Q} U_r) \sqrt{\det(\hat{Q}^\dagger)}]\}, \quad (2)$$

with $\hat{Q} = \exp[i2\pi \hat{x} \hat{y} / (N_x N_y)]$. \hat{x} (N_x) and \hat{y} (N_y) are the coordinate operator (sample size) along x and y directions, respectively. This definition makes use of the biorthogonal bases^{20,21,38,64}, which is different from Hermitian cases.

Next, let us prove that the pseudoanti-Hermiticity²⁴ [$H = -\eta H^\dagger \eta$, where the operator matrix η is a real diagonal matrix with $\eta = \eta^{-1}$] guarantees the quantization of the quadrupole moment Q_{xy} . The quantization of Q_{xy} is protected by the pseudoanti-Hermiticity instead of the chiral symmetry or particle-hole symmetry in Hermitian systems. Similar to the previous study⁵⁸, one obtains

$$\begin{aligned} \det(U_l^\dagger \hat{Q} U_r) &= \det[U_l^\dagger (\hat{Q} - \mathbb{I} + \mathbb{I}) U_r] \\ &= \det[\mathbb{I} + U_l^\dagger (\hat{Q} - \mathbb{I}) U_r] \\ &= \det[\mathbb{I} + (\hat{Q} - \mathbb{I}) U_r U_l^\dagger], \end{aligned} \quad (3)$$

by using the Sylvester's determinant identity⁵⁸ $\det(\mathbb{I} + AB) = \det(\mathbb{I} + BA)$. Biorthogonality-normalization relations indicate

$$\mathbf{RL}^\dagger = \begin{pmatrix} U_r & V_r \end{pmatrix} \begin{pmatrix} U_l^\dagger \\ V_l^\dagger \end{pmatrix} = \mathbb{I}. \quad (4)$$

Thus, one has $U_r U_l^\dagger = \mathbb{I} - V_r V_l^\dagger$. Noticing $V_l^\dagger V_r = \mathbb{I}$, one

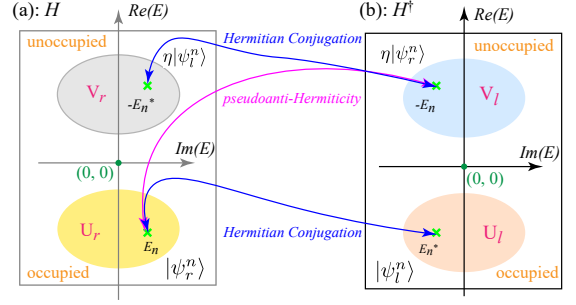


FIG. 1: (Color online). The relationship between n th eigenvalues E_n , E_n^* , $-E_n^*$, and $-E_n$. The corresponding eigenvectors are $|\psi_r^n\rangle$, $|\psi_l^n\rangle$, $\eta|\psi_l^n\rangle$, and $\eta|\psi_r^n\rangle$. (a) E_n and $-E_n^*$ are the eigenvalues of H . (b) E_n^* and $-E_n$ are the eigenvalues of H^\dagger . E_n ($-E_n$) and E_n^* ($-E_n^*$) are connected by the Hermitian conjugation. The Hermitian conjugation corresponds to the transformation between Hamiltonian H and H^\dagger , in which $|\psi_r^n\rangle$ will transform into $|\psi_l^n\rangle$. E_n (E_n^*) and $-E_n$ ($-E_n^*$) are correlated by pseudoanti-Hermiticity. We define the occupied ($Re[E] < 0$) and unoccupied ($Re[E] > 0$) conditions with the help of line gap along axis $Re[E]$. The matrices constructed by the occupied (unoccupied) standard right and left eigenvectors are marked as U_r (V_r) and U_l (V_l), respectively.

obtains:

$$\begin{aligned} \det(U_l^\dagger \hat{Q} U_r) &= \det[\mathbb{I} + (\hat{Q} - \mathbb{I})(\mathbb{I} - V_r V_l^\dagger)] \\ &= \det[\hat{Q} - (\hat{Q} - \mathbb{I}) V_r V_l^\dagger] \\ &= \det[\mathbb{I} + (\hat{Q}^\dagger - \mathbb{I}) V_r V_l^\dagger] \det(\hat{Q}) \\ &= \det(V_l^\dagger \hat{Q}^\dagger V_r) \det(\hat{Q}). \end{aligned} \quad (5)$$

After considering the pseudoanti-Hermiticity $\eta H \eta = -H^\dagger$ and Eq. (1), one has

$$-H^\dagger[\eta|\psi_r^n\rangle] = E_n[\eta|\psi_r^n\rangle], \quad -H[\eta|\psi_l^n\rangle] = E_n^*[\eta|\psi_l^n\rangle]. \quad (6)$$

Comparing Eq. (6) with Eq. (1), one can find that $\eta|\psi_r^n\rangle$ and $\eta|\psi_l^n\rangle$ are the standard left and right eigenvectors with the corresponding eigenvalues $-E_n$ and $-E_n^*$, respectively. That is to say, if E_n (E_n^*) is the eigenvalue of H (H^\dagger), η ensures that it has a corresponding partner $-E_n$ ($-E_n^*$), which is the eigenvalue of H^\dagger (H). The relationships between different eigenvalues and eigenvectors of H and H^\dagger are illustrated in Fig. 1. We have to point out that the Hermitian conjugation transformation used in this paper corresponds to the transformation between Hamiltonian H and H^\dagger . Thus, $|\psi_r^n\rangle$ ($\eta|\psi_l^n\rangle$) will transform into $|\psi_l^n\rangle$ ($\eta|\psi_r^n\rangle$) under such a transformation, which is called Hermitian conjugation only for simplicity.

Provided that $Re[E_n] < 0$, the following relations $|\psi_r^n\rangle \in U_r$, $|\psi_l^n\rangle \in U_l$, $\eta|\psi_r^n\rangle \in V_l$, and $\eta|\psi_l^n\rangle \in V_r$ can be obtained. These relations manifest that $\eta U_r = V_l$ as well as $\eta U_l = V_r$, and Eq. (5) can be rewritten as:

$$\begin{aligned} \det(U_l^\dagger \hat{Q} U_r) &= \det(V_l^\dagger \hat{Q}^\dagger V_r) \det(\hat{Q}) \\ &= \det(U_r^\dagger \eta \hat{Q}^\dagger \eta U_l) \det(\hat{Q}). \end{aligned} \quad (7)$$

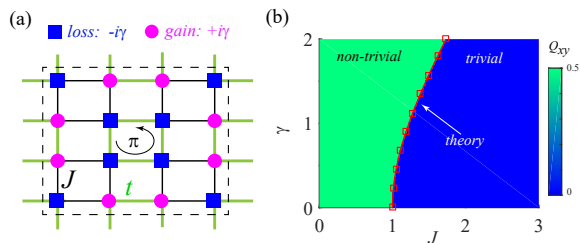


FIG. 2: (Color online). (a) Schematic diagram of the tight-binding model. The blue square (pink circle) represents the sites with loss $-i\gamma$ (gain $i\gamma$). The green and black solid lines show the nearest hopping with strength t and J , respectively. The dashed box is the primitive cell. π flux is also considered. (b) The quadrupole moment Q_{xy} versus J and γ . The red solid line is obtained based on the theoretical analysis. In all our calculation of Q_{xy} , the periodic boundary condition is adopted with sample size $N = 40$.

Since η is a real diagonal matrix and \hat{Q} is a unitary-diagonal matrix, one obtains $[\eta, \hat{Q}] = 0$ and $\hat{Q}^\dagger \hat{Q} = \mathbb{I}$. Thus,

$$\begin{aligned} \det(U_l^\dagger \hat{Q} U_r) \sqrt{\det(\hat{Q}^\dagger)} &= \det(U_r^\dagger \hat{Q}^\dagger U_l) \sqrt{\det(\hat{Q})} \\ &= [\det(U_l^\dagger \hat{Q} U_r) \sqrt{\det(\hat{Q}^\dagger)}]^\dagger. \end{aligned} \quad (8)$$

Therefore, $\det(U_l^\dagger \hat{Q} U_r) \sqrt{\det(\hat{Q}^\dagger)}$ is a real number, and Q_{xy} should be quantized to 0 or 0.5 as expected.

B. Model

We consider a square-lattice model protected by the pseudoanti-Hermiticity as an example. The primitive cell contains 16 sites, as shown in Fig. 2(a). It holds the pseudoanti-Hermiticity η , and the Hamiltonian reads²⁴:

$$\mathcal{H} = \sum_n i(\gamma + \varepsilon_n) \eta_n a_n^\dagger a_n + \sum_{\langle nm \rangle} t_{nm} e^{i\phi_{nm}} a_n^\dagger a_m \quad (9)$$

where t_{nm} (J or t) represents the nearest-neighbor hopping strength between sites n and m with the lattice constant $a_0 = 1$. J (t) corresponds to the black (green) solid lines in Fig. 2(a). η_n represents the diagonal element $\eta(n, n)$ with the operator matrix of pseudoanti-Hermiticity $\eta = \sigma_z \sigma_z \sigma_z \sigma_z$. a_n^\dagger (a_n) is the creation (annihilation) operator of site n . The magnetic flux⁶⁵ is determined by $\phi_{nm} = \frac{e}{\hbar} \int \mathbf{A} \cdot d\mathbf{l}$ with the vector potential $\mathbf{A} = (-By, 0, 0)$, and $d\mathbf{l}$ is the vector between n and m sites. We fix $\phi = a_0^2 B e / \hbar = \pi$ and $t = 1$ for simplicity. γ denotes gain or loss strength marked in different colors, which is illustrated in Fig. 2(a).

To maintain the pseudoanti-Hermiticity symmetry, the gain and loss disorder in one primitive cell is equivalent with $\varepsilon_n = \varepsilon$. For different primitive cells, ε is determined by Anderson disorder⁶⁶ with uniformly distributed $\varepsilon \in$

$[-W/2, W/2]$, where W is the disorder strength. Note that the system is set under half-filling conditions, i.e., the Fermi energy equals zero hereafter.

III. NUMERICAL RESULTS

This section illuminates that the real space topological invariant Q_{xy} is a powerful tool to identify the higher-order topological nontrivial/trivial phases even when the non-Hermitian appears. We also investigate the disorder effect in the corresponding non-Hermitian systems.

A. Q_{xy} as an indicator of non-Hermitian HOTI

Based on the quadrupole moment Q_{xy} calculation under the periodic boundary condition, we first obtain a phase diagram of non-Hermitian Hamiltonian in Eq. (9) with $W = 0$. As plotted in Fig. 2(b), Q_{xy} in the green region equals to 0.5 (nontrivial) and changes into zero (trivial) in the blue area. The evolution of Q_{xy} clearly shows the phase boundary shift between topological nontrivial and trivial phases by varying non-Hermitian strength γ . The red square solid line corresponds to the theoretically predicted phase boundary²⁴ with $\gamma^2 = 2(J^2 - 1^2)$. Specifically, one can easily find that these two-phase boundaries obtained by different methods coincide perfectly.

To better understand the nontrivial phase mentioned above, we analyze $Re[E]$ (blue) and $Im[E]$ (red) versus J under the periodic boundary condition as well as the open one for $\gamma = 1$. Theoretically, the bulk gap closes and reopens at $J = \sqrt{3/2} \approx 1.225$ for $\gamma = 1$. It consists with the plot of $Re[E]$ versus J under the periodic boundary condition (see Fig. 3(a)). Meanwhile, Q_{xy} versus J curve (see Fig. 3(b)) shows that Q_{xy} jumps

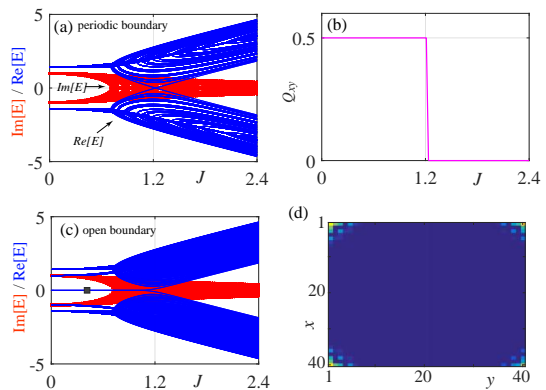


FIG. 3: (Color online). (a) The plot of the real $Re[E]$ (image $Im[E]$) part of the eigenvalue E versus J , marked in blue (red). (b) Q_{xy} versus J . (c) The same with (a), except the open boundary is adopted. (d) A typical plot of the wavefunction, which is marked by black square shown in (c). We fix $\gamma = 1$ in our calculation.

from 0.5 to 0 at $J \approx \sqrt{3/2}$, which signals that the bulk gap closing induces a topological phase transition. In order to clarify that $Q_{xy} = 0.5$ determines the existence of non-Hermitian HOTI, we plot $Re[E]$ (blue) and $Im[E]$ (red) versus J under the open boundary condition. Fig. 3(c) suggests that the zero-energy modes appear when $J < \sqrt{3/2}$, and the fourfold-degeneracy corner states emerge [see Fig. 3(d)]. The corner states' energy deviation from $Re[E] = 0$ for $J \approx \sqrt{3/2}$ is due to the finite size effect. In short, the non-Hermitian HOTI exists when $J < \sqrt{3/2}$, and Q_{xy} clearly distinguishes such a phase from the trivial one.

To sum up, we show that the pseudoanti-Hermiticity symmetry protected quadrupole moment Q_{xy} (defined as Eq. (2)) can be utilized to distinguish non-Hermitian HOTI.

B. Non-Hermitian HOTAI

Subsequently, by considering disorder with pseudoanti-Hermiticity symmetry, we investigate the disorder-induced phase transition in non-Hermitian systems. Notably, we examine the existence of the non-Hermitian HOTAI.

The evolution of Q_{xy} by increasing disorder strength W with $J = 0.5$ is plotted in Fig. 4(a). Under the clean limit of $W = 0$, the system is non-Hermitian HOTI with $Q_{xy} = 0.5$. Unless otherwise specified, the disorder in numerical calculations holds the pseudoanti-Hermiticity symmetry η . We find that the average quadrupole moment Q_{xy} (solid blue line) is quantized to 0.5 for $W < 3$. Meanwhile, the zero-energy modes in the bulk gap [see Fig. 4(b)] as well as the corresponding wavefunction of corner states [see Fig. 4(c)] indicate that non-Hermitian HOTI is robust against disorder. Significantly, if the disorder-induced HOTAI emerges in such a system, it can also be identified by the quantization of Q_{xy} .

Next, we investigate the disorder-induced topological phase transition for $J = 1.26$, as shown in Figs. 4(d)-(f). The sample is normal insulator (NI) with $Q_{xy} = 0$ and without the zero-energy states under clean limit since $1.26 > \sqrt{3/2}$. With the increasing of disorder strength W , the average quadrupole moment Q_{xy} jumps from 0 to 0.5 [see Fig. 4(d)]. Further, the $Q_{xy} = 0.5$ plateau holds for disorder strength near $W \approx 2.5$. Taking $W = 2.5$ as an example, as shown in Fig. 4(e) and (f), we find the in-gap zero-energy states, as well as the corner states, exist. Different from those in Fig. 4(b) and (c), the four zero-energy modes in the bulk gap are no longer strictly degenerate, and the average wavefunction slightly penetrates into the bulk. These features should be related to the enhancement of coupling strength between four corner modes induced by disorder. However, the main property of the corner states in the bulk gap is still reserved. Therefore, it is reasonable to conclude that the region with $Q_{xy} = 0.5$ in Fig. 4(d) belongs to the non-Hermitian HOTAI.

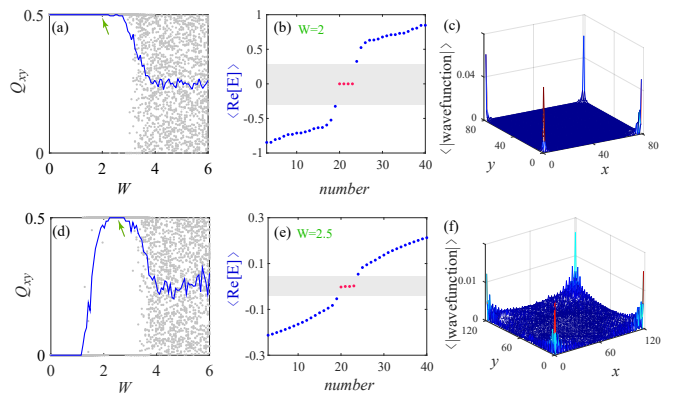


FIG. 4: (Color online). (a) The evolution of quadrupole moment Q_{xy} by increasing disorder strength W with $J = 0.5$. The gray dots are Q_{xy} for each disordered sample, and the blue solid line is the average. (b) and (c) are the average energy $Re[E]$ and wavefunction [red dots marked in (b)] for $W = 2$. (d)-(f) is similar to (a)-(c) except $J = 1.26$ and $W = 2.5$. Q_{xy} is calculated under periodic boundary condition. Only several eigenvalues close to $Re[E] = 0$ are plotted in (b) and (e).

We also notice that Q_{xy} cannot be quantized under strong disorder $W > 3$ in both Fig. 4(a) and (d). The distribution of Q_{xy} for each sample seems random, and the average quadrupole moment approximately equals 0.25. This behavior is also different from that in Hermitian HOTAI cases^{57,58}, where topological invariant Q_{xy} decreases to zero under strong disorder. In order to explain the unquantized Q_{xy} and further ensure the existence of the non-Hermitian HOTAI, we plot the evolution of $\langle Re[E] \rangle$ with the increase of W under the periodic boundary condition [see Fig. 5(a) and (b)]. Here, $\langle Re[E] \rangle$ is the average of $Re[E]$.

For $J = 0.5$ (nontrivial case), the bulk gap gradually decreases and finally closes with the increasing disorder strength W [see Fig. 5(a)]. Q_{xy} is unquantized when $W > 3$. Similarly, as shown in Fig. 5(b), we consider trivial case with $J = 1.26$. The bulk gap closes and reopens with an increase of disorder strength. Meanwhile, Q_{xy} jumps from 0 to 0.5, which strongly suggests the occurrence of the phase transition from NI to non-Hermitian HOTAI. Continuing to increase disorder strength for $W > 3$, the bulk gap gradually reduces and closes. The quadrupole moment Q_{xy} deviates from the quantized value accordingly.

In order to better understand the deviation of Q_{xy} from the quantized value, we concentrate on the average $Re[E]$ as well as the average wavefunction with $W = 4.5$. By setting $J = 1.26$, the bulk gap disappears, and the average wavefunction extends into the bulk [see Figs. 5(c)-(d)]. Further, a series of $\langle Re[E] \rangle = 0$ states appear, which are named as the gapless phase²⁷. The existence of states with $\langle Re[E] \rangle = 0$ for the gapless phase is reasonable. Taking $H = \begin{bmatrix} i(\gamma + W) & t \\ t & -i(\gamma + W) \end{bmatrix}$ as an intu-

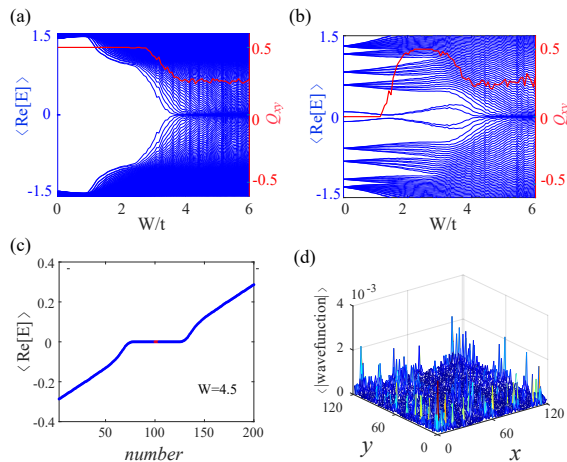


FIG. 5: (Color online). (a) The evolution of $\text{Re}[E]$ with the increase of W . The red line shows Q_{xy} for each disordered sample. Here, $J = 0.5$. (b) is similar to (a) with $J = 1.26$. (c) shows $\text{Re}[E]$ with disorder strength $W = 4.5$. Only several eigenvalues close to $\text{Re}[E] = 0$ are plotted. (d) is the average wavefunction of the red dots in (c). (a) and (b) are calculated under periodic boundary condition with sample size $N = 40$. (c)-(d) are calculated under open boundary condition with $J = 1.26$ and $N = 120$.

itive example, its eigenvalues are $E = \pm\sqrt{t^2 - (\gamma + W)^2}$. For fixed t and γ , $\langle \text{Re}[E] \rangle$ tends to zero when W is strong enough. For such a case, we have to emphasize that the half-filling condition is not well-defined because of the existence of states with $\text{Re}[E] = 0$ [see Fig. 5(c)]. However, the accuracy limitation in the numerical calculation slightly lifts these zero modes' degeneracy, which leads to an incorrect half-filling condition. Thus, the specific transformation between the occupied (U_r, U_l) and unoccupied states (V_r, V_l) cannot hold [see Fig. 1]. The unquantized Q_{xy} can be considered as a signal for the existence of the gapless phase.

These findings indicate that the quantized Q_{xy} requires not only symmetry but also the existence of bulk gap along $\text{Re}[E]$. When such a bulk gap disappears, the quantization of Q_{xy} is not available. Significantly, the absence of bulk gap distinguishes the zero-energy modes in Fig. 5(c) from the non-Hermitian HOTAI shown in Fig. 4(e). Moreover, the evolution of eigenvalues versus W also strengthens the existence of non-Hermitian HOTAI shown in Figs. 4(d)-(f).

IV. SUMMARY AND DISCUSSION

In summary, based on the real space topological invariant [quadrupole moment in the frame of non-Hermitian Hamiltonian], we studied the disorder-induced HOTAI in non-Hermitian systems, which is protected by the pseudoanti-Hermiticity. First, we demonstrated that the quadrupole moment Q_{xy} can be quantized to 0 or 0.5 by utilizing the biorthogonal bases. It is found that

the quadrupole moment Q_{xy} can be utilized to distinguish non-Hermitian HOTI ($Q_{xy} = 0.5$) from the trivial ones ($Q_{xy} \neq 0.5$). Then, with the help of Q_{xy} , we uncovered the disorder-induced phase transition in such a non-Hermitian system and demonstrated the existence of non-Hermitian HOTAI.

The real space topological invariant Q_{xy} is a powerful tool to characterize non-Hermitian HOTI. In the appendix, we give another non-Hermitian HOTI without pseudoanti-Hermiticity symmetry and with NHSE to further declare the scope of application of Q_{xy} . We show that the quantized Q_{xy} is also available for samples with sublattice symmetry combined with a non-unitary transformation. Besides, NHSE has no specific influence on the topological invariant Q_{xy} , except by considering the non-Bloch band theory²⁰⁻²³. Theoretically, the chiral symmetry and particle-hole symmetry in Altland-Zirnbauer classification for Hermitian cases should be replaced by specific symmetries in 38-fold classification for non-Hermitian cases²⁷. In addition to the pseudoanti-Hermiticity and sublattice symmetry reported in this paper, other symmetries in non-Hermitian systems may also be able to be utilized to ensure the quantization of Q_{xy} . Further, the line gap along $\text{Im}[E]$ will also influence the characterization of Q_{xy} . A much careful investigation can complete the understanding of topological features of non-Hermitian systems.

acknowledgement

We are grateful to Yue-Ran Ding, Zibo Wang, Ming Gong, and especially Qiang Wei for insightful discussion. This work is financially supported by the National Basic Research Program of China No. 2019YFA0308403, National Natural Science Foundation of China No. 11822407, and a Project Funded by the Priority Academic Program Development of Jiangsu Higher Education Institutions.

Appendix A: Influence of NHSE and the sublattice symmetry protected quadrupole moment in non-Hermitian systems

In the appendix, we investigate applicability of the quadrupole moment Q_{xy} for other symmetries, and the NHSE is also considered. As an example, we focus on the sublattice symmetry protected non-Hermitian HOTI with NHSE. Although sublattice symmetry itself cannot ensure the quantization of Q_{xy} , we prove that there is another transformation, which connects H to H^\dagger . The combination of these two transformations is similar to pseudoanti-Hermiticity, which connects H to $-H^\dagger$. Therefore, the quantization of Q_{xy} is still available even in the presence of disorder. Significantly, the quadrupole moment Q_{xy} defined in real space is also applicable for systems with NHSE.

1. Quantization of Q_{xy} for systems with sublattice symmetry and NHSE

Following the previous study, the Hamiltonian for non-Hermitian HOTI with NHSE reads²⁵:

$$\begin{aligned} H(\mathbf{k}) &= H_0 + H(k_x) + H(k_y) \\ &= t(\tau_x\sigma_0 + \tau_y\sigma_y) + i\gamma(\tau_y\sigma_x - \tau_y\sigma_z) \\ &\quad + \lambda \cos(k_x) \tau_x\sigma_0 - \lambda \sin(k_x) \tau_y\sigma_z \\ &\quad + \lambda \cos(k_y) \tau_y\sigma_y + \lambda \sin(k_y) \tau_y\sigma_x, \end{aligned} \quad (\text{A1})$$

where $\tau_{x/y/z}$ and $\sigma_{x/y/z}$ are the Pauli matrices. τ_0 and σ_0 are the identity matrices. γ denotes the non-Hermitian strength. For simplicity, we fix $\gamma = 0.4$. H_0 represents the intra primitive cell hopping matrix. $H(k_x)$ and $H(k_y)$ show the hopping matrices between the nearest neighbor primitive cells along x and y directions, respectively.

Eq. (A1) has the sublattice symmetry $SH(\mathbf{k})S = -H(\mathbf{k})$ with $S = \tau_z\sigma_0$. Sublattice symmetry operator S connects $U_{l/r}$ to $V_{l/r}$ and vice versa. Eq. (5) implies that S itself cannot ensure the quantization of Q_{xy} since $U_l^\dagger U_l \neq \mathbb{I}$ in non-Hermitian systems⁵⁸. The quantization of Q_{xy} demands another matrix A which connects H with H^\dagger . In addition, A has to commute with \hat{Q} and satisfies $A^\dagger = A$. Moreover, the unbalanced hoppings along both x and y directions suggest the existence of NHSE. In terms of two requirements above, we prove that there is a matrix, which transforms H to H^\dagger after eliminating the NHSE. Thus, the quantized Q_{xy} is ensured.

In the following, we detail the derivation. The matrix forms of H_0 , $H(k_x)$, and $H(k_y)$ are:

$$H_0 \equiv T_0 = \begin{bmatrix} 0 & 0 & t-\gamma & -t+\gamma \\ 0 & 0 & t+\gamma & t+\gamma \\ t+\gamma & t-\gamma & 0 & 0 \\ -t-\gamma & t-\gamma & 0 & 0 \end{bmatrix}, \quad (\text{A2})$$

$$H(k_x) = T_x e^{ik_x} + T_x^\dagger e^{-ik_x},$$

$$H(k_y) = T_y e^{ik_y} + T_y^\dagger e^{-ik_y},$$

$$\text{with } T_x = \begin{bmatrix} 0 & 0 & \lambda & 0 \\ 0 & 0 & 0 & 0 \\ 0 & 0 & 0 & 0 \\ 0 & \lambda & 0 & 0 \end{bmatrix} \text{ and } T_y = \begin{bmatrix} 0 & 0 & 0 & -\lambda \\ 0 & 0 & 0 & 0 \\ 0 & \lambda & 0 & 0 \\ 0 & 0 & 0 & 0 \end{bmatrix}. T_{x/y}^\dagger \text{ is}$$

the hermitian conjugation of $T_{x/y}$. Due to the NHSE, the correct phase diagram is available by combining the non-Bloch band theory under periodic boundary condition. The replacement of momentum²⁵ $k_{x/y} \rightarrow \tilde{k}_{x/y} + ik_0$ leads to

$$\begin{aligned} H(\tilde{k}_x) &= \beta T_x e^{i\tilde{k}_x} + \beta^{-1} T_x^\dagger e^{-i\tilde{k}_x}, \\ H(\tilde{k}_y) &= \beta T_y e^{i\tilde{k}_y} + \beta^{-1} T_y^\dagger e^{-i\tilde{k}_y}, \\ H^\dagger(\tilde{k}_x) &= \beta T_x^\dagger e^{-i\tilde{k}_x} + \beta^{-1} T_x e^{i\tilde{k}_x}, \\ H^\dagger(\tilde{k}_y) &= \beta T_y^\dagger e^{-i\tilde{k}_y} + \beta^{-1} T_y e^{i\tilde{k}_y}, \end{aligned} \quad (\text{A3})$$

where $\beta = e^{-k_0} = \sqrt{|(t-\gamma)/(t+\gamma)|}$. Such replacement leaves H_0 unchanged.

Matrix A should connect $H(\tilde{\mathbf{k}})$ with $H^\dagger(\tilde{\mathbf{k}})$. Thus:

$$A = \begin{bmatrix} \frac{t+\gamma}{t-\gamma} & 0 & 0 & 0 \\ 0 & \frac{t-\gamma}{t+\gamma} & 0 & 0 \\ 0 & 0 & 1 & 0 \\ 0 & 0 & 0 & 1 \end{bmatrix}. \quad (\text{A4})$$

It transforms H_0 , $H(\tilde{k}_x)$ and $H(\tilde{k}_y)$ as follows:

$$\begin{aligned} AH_0A^{-1} &= H_0^\dagger, \\ AH(\tilde{k}_x)A^{-1} &= a_1\beta T_x e^{i\tilde{k}_x} + a_2\beta^{-1} T_x^\dagger e^{-i\tilde{k}_x}, \\ AH(\tilde{k}_y)A^{-1} &= a_1\beta T_y e^{i\tilde{k}_y} + a_2\beta^{-1} T_y^\dagger e^{-i\tilde{k}_y}, \end{aligned} \quad (\text{A5})$$

with $a_1 = (t+\gamma)/(t-\gamma)$, and $a_2 = (t-\gamma)/(t+\gamma)$. Since $\beta = \sqrt{|(t-\gamma)/(t+\gamma)|}$, $a_1\beta$ and $a_2\beta^{-1}$ have two conditions to eliminate the absolute value sign of β . Two cases are analyzed as below:

case 1: For $\frac{t-\gamma}{t+\gamma} > 0$, $\beta = \sqrt{\frac{t-\gamma}{t+\gamma}} = \sqrt{\frac{t-\gamma}{t+\gamma}}$. The multiplication is available

$$a_1\beta = \beta^{-1}, \quad a_2\beta^{-1} = \beta. \quad (\text{A6})$$

It leads to

$$AH(\tilde{k}_x, \tilde{k}_y)A^{-1} = H^\dagger(\tilde{k}_x, \tilde{k}_y). \quad (\text{A7})$$

case 2: For $\frac{t-\gamma}{t+\gamma} < 0$, $\beta = \sqrt{\frac{t-\gamma}{t+\gamma}} = \sqrt{\frac{\gamma-t}{t+\gamma}}$. Thus,

$$a_1\beta = -\beta^{-1}, \quad a_2\beta^{-1} = -\beta. \quad (\text{A8})$$

One obtains

$$AH(\tilde{k}_x, \tilde{k}_y)A^{-1} = H^\dagger(\tilde{k}_x + \pi, \tilde{k}_y + \pi). \quad (\text{A9})$$

To make it more intuitive, let's analyze the transformation of $H(\tilde{k}_x, \tilde{k}_y)$ in the real space for a square sample with sample size $N \times N$. We suppose there is a diagonal matrix

$$A_R = \text{diag}(\text{diag}(A_1), \text{diag}(A_2), \dots, \text{diag}(A_i), \dots), \quad (\text{A10})$$

with $A_i = \text{diag}(\text{diag}(A_i))$. diag represents the diagonal. A_i is the construction block of A_R , which satisfies $A_i = \pm A$. To ensure $A_R H A_R^{-1} = H^\dagger$, the following relations should hold

$$\begin{aligned} A_i T_0 A_i^{-1} &= T_0^\dagger; \\ A_i \beta T_x A_j^{-1} &= \beta^{-1} T_x, \quad A_i \beta T_y A_j^{-1} = \beta^{-1} T_y; \\ A_i \beta^{-1} T_x^\dagger A_j^{-1} &= \beta T_x^\dagger, \quad A_i \beta^{-1} T_y^\dagger A_j^{-1} = \beta T_y^\dagger; \end{aligned} \quad (\text{A11})$$

where the corresponding hopping matrix between i and j primitive cells is clarified in the equation. For all the

$i \in [1, N^2]$, $A_i = A$ when $\frac{t-\gamma}{t+\gamma} > 0$. It ensures $A_R H A_R^{-1} = H^\dagger$.

When $\frac{t-\gamma}{t+\gamma} < 0$, we assume $A_{i \in \text{odd}} = -A_{j \in \text{even}}$ with $i, j \in [1, N] + kN$ and $k \in [0, N-1]$. For $i \in [1, N] + kN$ and $j \in [N+1, 2N] + kN$ with $k \in [0, N-2]$, we require $A_i = -A_j$. The above limits also preserve $A_R H A_R^{-1} = H^\dagger$. Furthermore, we notice that A_R is a diagonal matrix as expected for these two cases, and it commutes with \hat{Q} . Significantly, $A_R^\dagger = A_R$ is also satisfied.

Again, we take Eq. (1) as an example and suppose $\text{Re}(E_n) < 0$. A_R satisfies $A_R H A_R^{-1} = H^\dagger$, which means:

$$\begin{aligned} H^\dagger[A_R^{-1}|\psi_r^n\rangle] &= E_n[A_R^{-1}|\psi_r^n\rangle], \\ H[A_R|\psi_l^n\rangle] &= E_n^*[A_R|\psi_l^n\rangle]. \end{aligned} \quad (\text{A12})$$

one obtains $A_R^{-1}|\psi_r^n\rangle \in U_l$ and $A_R|\psi_l^n\rangle \in U_r$. Noticing that the replacement $\mathbf{k} \rightarrow \tilde{\mathbf{k}} + ik_0$ maintains the sublattice symmetry S , the relationship $SHS = -H$ still holds with $S = S^{-1}$. Thus:

$$\begin{aligned} -H[S|\psi_r^n\rangle] &= E_n[S|\psi_r^n\rangle], \\ -H^\dagger[S|\psi_l^n\rangle] &= E_n^*[S|\psi_l^n\rangle]. \end{aligned} \quad (\text{A13})$$

It is obvious that $S|\psi_r^n\rangle \in V_r$ and $S|\psi_l^n\rangle \in V_l$.

The corresponding relations between different states are shown in Fig. A1(a) and (b). For state $|\psi_r^n\rangle$ with eigenvalue E_n , A_R will transform $|\psi_r^n\rangle \in U_r$ to $A_R^{-1}|\psi_r^n\rangle \in U_l$ with E_n unchanged [the black solid line in Fig. A1(a) and (b)]. Then, the sublattice symmetry S will transform $A_R^{-1}|\psi_r^n\rangle \in U_l$ to $SA_R^{-1}|\psi_r^n\rangle \in V_l$ with $E_n \rightarrow -E_n$ [the cyan solid line]. The combination of S and A_R will connect $|\psi_r^n\rangle \in U_r$ to $SA_R^{-1}|\psi_r^n\rangle \in V_l$ [the pink solid line], which means SA_R^{-1} connects H to $-H^\dagger$.

We emphasize that the Hermitian-conjugation correlates E_n (eigenvalue of H) with E_n^* (eigenvalue of H^\dagger), which is different from the transformation A_R . A_R correlates E_n (eigenvalue of H) with E_n (eigenvalue of H^\dagger). It means that the n th eigenvalue of H^\dagger (E_n) should be a real number. Otherwise, E_n must have a complex conjugate partner E_n^* , as shown in Fig. A1(b).

To sum up, we obtain the following transformations:

$$\begin{cases} SHS = -H \\ A_R H A_R^{-1} = H^\dagger \end{cases} \Rightarrow \begin{cases} V_{l/r} = S U_{l/r} \\ U_l = A_R^{-1} U_r \\ U_r = A_R U_l \end{cases}. \quad (\text{A14})$$

For non-Hermitian systems with sublattice symmetry, the quantization of Q_{xy} is not guaranteed since $V_{l/r} = S U_{l/r}$ cannot ensure that $\det(U_r^\dagger \hat{Q}^\dagger U_l) \sqrt{\det(\hat{Q})}$ is a real number. However, one can prove the quantization of Q_{xy} is confirmed after combining S and A_R . Following

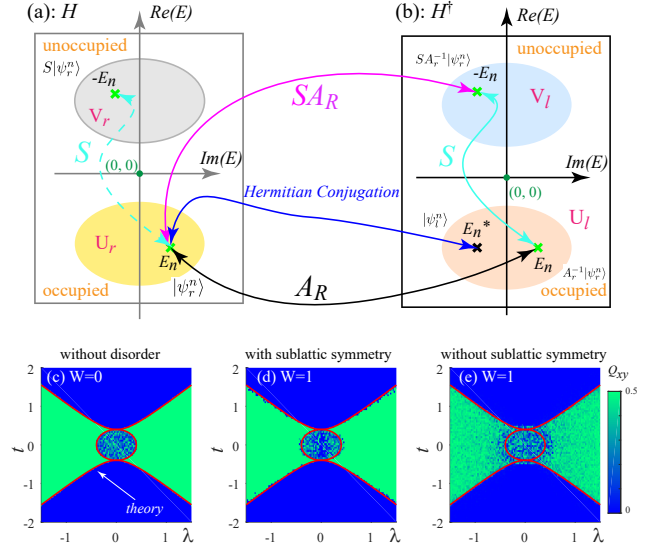


FIG. A1: (Color online). (a) and (b) are similar to those in Fig. 1, except that the transformation operator is changed. S corresponds to the sublattice symmetry. A_R is a matrix defined in the appendix. (c)-(e) The phase diagram of non-Hermitian Hamiltonian Eq. (A1) with sublattice symmetry. The quadrupole moment Q_{xy} versus t and λ . The blue regions represent the topologically trivial phase with $Q_{xy} = 0$, while the green regions represent the non-Hermitian HOTI with $Q_{xy} = 0.5$. The middle regions inside the ellipse represents the gapless states [Q_{xy} lies between 0 and 0.5]. The phase boundaries²⁵ (red line) are determined by $t^2 = \gamma^2 + \lambda^2$ and $t^2 = \gamma^2 - \lambda^2$ with $\gamma = 0.4$. (c) with sublattice symmetry and without disorder $W = 0$. (d) with sublattice symmetry and disorder strength $W = 1$. (e) is similar to (d), except that the sublattice symmetry broken disorder is considered.

Eq. (5), we have:

$$\begin{aligned} \det(U_l^\dagger \hat{Q} U_r) &= \det(V_l^\dagger \hat{Q} V_r) \det(\hat{Q}) \\ &= \det(U_l^\dagger S^\dagger \hat{Q}^\dagger S U_r) \det(\hat{Q}) \\ &= \det(U_l^\dagger \hat{Q}^\dagger U_r) \det(\hat{Q}) \\ &= \det(U_r^\dagger A_R^{-1 \dagger} \hat{Q}^\dagger A_R U_l) \det(\hat{Q}) \\ &= \det(U_r^\dagger A_R^{-1} \hat{Q}^\dagger A_R U_l) \det(\hat{Q}) \\ &= \det(U_r^\dagger \hat{Q}^\dagger U_l) \det(\hat{Q}), \end{aligned} \quad (\text{A15})$$

which means

$$\det(U_l^\dagger \hat{Q} U_r) \sqrt{\det(\hat{Q}^\dagger)} = [\det(U_l^\dagger \hat{Q} U_r) \sqrt{\det(\hat{Q}^\dagger)}]^\dagger. \quad (\text{A16})$$

Thus, similar as Eq. (8), the quantization of Q_{xy} to 0 or 0.5 is ensured as expected.

2. Numerical results

We check that the quantized Q_{xy} can be used to predict a correct phase diagram of such a non-Hermitian HOTI.

The plots of Q_{xy} versus γ and t are given in Fig. A1. To eliminate the influence of NHSE, the numerical calculation is based on $H(\tilde{k}_x, \tilde{k}_y)$ instead of $H(k_x, k_y)$. The periodic boundary condition is also adopted.

When the disorder is absent, the quantized Q_{xy} perfectly captures the existence of non-Hermitian HOTI. As shown in Fig. A1(c), the solid red line is the theoretically predicted phase boundary. The regions with $Q_{xy} = 0.5$ fit the theoretical analysis quite well. We also notice that Q_{xy} shows different behaviors for different parameter regions. When $t^2 > \gamma^2 + \lambda^2$, one has $Q_{xy} = 0$, which is a NI. However, Q_{xy} is unquantized when $t^2 < \gamma^2 - \lambda^2$, and it seems to contradict with the symmetry-protected

quantization of Q_{xy} . Actually, it corresponds to the gapless phase.

Next, we study the influence of disorder effect on the quantization of Q_{xy} . Two kinds of disorder, which preserves or breaks the sublattice symmetry, are considered. In Fig. A1(d), the disorder is added to the hopping terms along y direction. Since the sublattice symmetry still holds, the quantized Q_{xy} is still available. On the other hand, the quantized Q_{xy} disappears [see Fig. A1(e)] when the on-site energy potential is adopted, which breaks the sublattice symmetry. These results are consistent with the previous analysis.

-
- * Electronic address: zqzhang2018@stu.suda.edu.cn
† Electronic address: jianghuaphy@suda.edu.cn
- ¹ M. Z. Hasan, and C. L. Kane, Colloquium: topological insulators, *Rev. Mod. Phys.* **82**, 3045 (2010).
 - ² J. E. Moore, The birth of topological insulators, *Nature* **464**, 194 (2010).
 - ³ X. L. Qi, and S. C. Zhang, Topological insulators and superconductors, *Rev. Mod. Phys.* **83**, 1057 (2011).
 - ⁴ B. A. Bernevig, T. L. Hughes, and S. C. Zhang, Quantum Spin Hall Effect and Topological Phase Transition in HgTe Quantum Wells, *Science* **314**, 1757 (2006).
 - ⁵ M. König, S. Wiedmann, C. Brüne, A. Roth, H. Buhmann, L. W. Molenkamp, X. L. Qi, and S. C. Zhang, Quantum Spin Hall Insulator State in HgTe Quantum Wells, *Science* **318**, 766 (2007).
 - ⁶ L. Trifunovic, and P. W. Brouwer, Higher-Order Bulk-Boundary Correspondence for Topological Crystalline Phases, *Phys. Rev. X* **9**, 011012 (2019).
 - ⁷ B. H. Yan, and C. Felser, Topological Materials: Weyl Semimetals, *Annu. Rev. Condens. Matter Phys.* **8**, 337 (2017).
 - ⁸ Z. K. Liu, B. Zhou, Y. Zhang, Z. J. Wang, H. M. Weng, D. Prabhakaran, S. K. Mo, Z. X. Shen, Z. Fang, X. Dai, Z. Hussain, and Y. L. Chen, Discovery of a Three-Dimensional Topological Dirac Semimetal, Na₃Bi, *Science* **343**, 864 (2014).
 - ⁹ J. Alicea, New directions in the pursuit of Majorana fermions in solid state systems, *Rep. Prog. Phys.* **75**, 076501 (2012).
 - ¹⁰ F. Tang, H. C. Po, A. Vishwanath, and X. G. Wan, Comprehensive search for topological materials using symmetry indicators, *Nature* **566**, 486 (2019).
 - ¹¹ T. T. Zhang, J. Jiang, Z. D. Song, H. Huang, Y. Q. He, Z. Fang, H. M. Weng, and C. Fang, Catalogue of topological electronic materials, *Nature* **566**, 475 (2019).
 - ¹² M. G. Vergniory, L. Elcoro, C. Felser, N. Regnault, B. A. Bernevig, and Z. J. Wang, The (High Quality) Topological Materials in the world, *Nature* **566**, 480 (2019).
 - ¹³ L. Fu, Topological Crystalline Insulators, *Phys. Rev. Lett.* **106**, 106802 (2011).
 - ¹⁴ Y. Ando, and L. Fu, Topological Crystalline Insulators and Topological Superconductors: From Concepts to Materials, *Annu. Rev. Condens. Matter Phys.* **6**, 361 (2015).
 - ¹⁵ Z. P. Gong, Y. Ashida, K. Kawabata, K. Takasan, S. Higashikawa, and M. Ueda, Topological Phases of Non-Hermitian Systems, *Phys. Rev. X* **8**, 031079 (2018).
 - ¹⁶ X. Y. Zhu, H. Q. Wang, S. K. Gupta, H. J. Zhang, B. Y. Xie, M. H. Lu, and Y. F. Chen Photonic non-Hermitian skin effect and non-Bloch bulk-boundary correspondence, *Phys. Rev. Research* **2**, 013280 (2020).
 - ¹⁷ Q. B. Zeng, and Y. Xu, Winding numbers and generalized mobility edges in non-Hermitian systems, *Phys. Rev. Research* **2**, 033052 (2020).
 - ¹⁸ K. Zhang, Z. S. Yang, and C. Fang, Correspondence between Winding Numbers and Skin Modes in Non-Hermitian Systems, *Phys. Rev. Lett.* **125**, 126402 (2020).
 - ¹⁹ N. Okuma, K. Kawabata, K. Shiozaki, and M. Sato, Topological Origin of Non-Hermitian Skin Effects, *Phys. Rev. Lett.* **124**, 086801 (2020).
 - ²⁰ S. Y. Yao, and Z. Wang, Edge States and Topological Invariants of Non-Hermitian Systems, *Phys Rev Lett.* **121**, 086803 (2018).
 - ²¹ S. Y. Yao, F. Song, and Z. Wang, Non-Hermitian Chern Bands, *Phys. Rev. Lett.* **121**, 136802 (2018).
 - ²² K. Yokomizo, and S. Murakami, Non-Bloch Band Theory of Non-Hermitian Systems, *Phys.Rev.Lett.* **123**, 066404 (2019).
 - ²³ K. Yokomizo, and S. Murakami, Non-Bloch Band Theory and Bulk-Edge Correspondence in Non-Hermitian Systems, *arXiv:2009.04220* (2020).
 - ²⁴ X.W. Luo, and C. W. Zhang, Higher-Order Topological Corner States Induced by Gain and Loss, *Phys. Rev. Lett.* **123**, 073601 (2019).
 - ²⁵ T. Liu, Y.R. Zhang, Q. Ai, Z. Gong, K. Kawabata, M. Ueda, and F. Nori, Second-order topological phases in non-Hermitian systems, *Phys. Rev. Lett.* **122**, 076801 (2019).
 - ²⁶ Y. Ashida, Z. P. Gong, and M. Ueda, Non-Hermitian Physics, *arXiv: 2006.01837* (2020).
 - ²⁷ K. Kawabata, K. Shiozaki, M. Ueda, and M. Sato, Symmetry and Topology in Non-Hermitian Physics, *Phys. Rev. X* **9**, 041015 (2019).
 - ²⁸ K. Kawabata, M. Sato, and K. Shiozaki, Higher-order non-Hermitian skin effect, *arXiv:2008.07237* (2020).
 - ²⁹ K. Zhang, Z. S. Yang, and C. Fang, Correspondence between winding numbers and skin modes in non-hermitian systems, *arXiv:1910.01131* (2020).
 - ³⁰ Y. F. Yi, and Z. S. Yang, Non-Hermitian Skin Modes Induced by On-Site Dissipations and Chiral Tunneling Effect, *Phys. Rev. Lett.* **125**, 186802 (2020).
 - ³¹ N. Okuma, and M. Sato, Quantum anomaly, non-

- Hermitian skin effects, and entanglement entropy in open systems, arXiv:2011.08175 (2020).
- ³² H. Jiang, L. J. Lang, C. Yang, S. L. Zhu, and S. Chen, Interplay of non-Hermitian skin effects and Anderson localization in nonreciprocal quasiperiodic lattices, *Phys. Rev. B* **100**, 054301 (2019).
- ³³ A. F. Tzortzakakis, K. G. Makris, E. N. Economou, Non-Hermitian disorder in two-dimensional optical lattices, *Phys. Rev. B* **101**, 014202 (2020).
- ³⁴ A. F. Tzortzakakis, K. G. Makris, S. Rotter, and E. N. Economou, Shape-preserving beam transmission through non-Hermitian disordered lattices, *Phys. Rev. A* **102**, 033504 (2020).
- ³⁵ C. C. Wanjura, M. Brunelli, A. Nunnenkamp, Correspondence between non-Hermitian topology and directional amplification in the presence of disorder, arXiv:2010.14513 (2020).
- ³⁶ A. F. Tzortzakakis, K. G. Makris, A. Szameit, and E. N. Economou, Non-Hermitian lattices with binary-disorder, arXiv:2007.08825 (2020)
- ³⁷ L. Z. Tang, L. F. Zhang, G. Q. Zhang, and D. W. Zhang, Topological Anderson insulators in two-dimensional non-Hermitian disordered systems, *Phys. Rev. A* **101**, 063612 (2020).
- ³⁸ H. F. Liu, Z. X. Su, Z.-Q. Zhang, and H. Jiang, Topological Anderson insulator in two-dimensional non-Hermitian systems, *Chinese Phys. B* **29**, 050502 (2020).
- ³⁹ D. W. Zhang, L. Z. Tang, L. J. Lang, H. Yan, and S. L. Zhu, Non-Hermitian Topological Anderson Insulators, *Sci. China-Phys. Mech. Astron.* **63**, 267062 (2020).
- ⁴⁰ X. W. Luo, and C. W. Zhang, Non-Hermitian Disorder-induced Topological insulators, arXiv:1912.10652 (2019).
- ⁴¹ C. Wang and X. R. Wang, Level statistics of extended states in random non-Hermitian Hamiltonians, *Phys. Rev. B* **101**, 165114 (2020).
- ⁴² X. L. Luo,¹ T. Ohtsuki, and R. Shindou, Universality classes of the Anderson Transitions Driven by non-Hermitian Disorder, arXiv:2011.07528.
- ⁴³ J. T. Song, and E. Prodan, AIII and BDI topological systems at strong disorder, *Phys. Rev. B* **89**, 224203 (2014).
- ⁴⁴ Z. Q. Zhang, C. Z. Chen, Y. J. Wu, H. Jiang, J. W. Liu, Q. F. Sun, and X. C. Xie, Chiral Interface States and Related Quantized Transport in Disordered Chern Insulators, *Phys. Rev. B* **103**, 075434 (2021).
- ⁴⁵ Z. X. Su, Y. Z. Kang, B. F. Zhang, Z. Q. Zhang and H. Jiang, Disorder induced phase transition in magnetic higher-order topological insulator: A machine learning study, *Chin. Phys. B* **28**, 117301 (2019).
- ⁴⁶ E. Prodan, Disordered topological insulators: a non-commutative geometry perspective, *Phys. A-Math. Theor.* **44**, 113001 (2011).
- ⁴⁷ Y. F. Zhang, Y. Y. Yang, Y. Ju, L. Sheng, R. Shen, D. N. Sheng, and D. Y. Xing, Coupling-matrix approach to the Chern number calculation in disordered systems, *Chin. Phys. B* **22** 117312 (2013).
- ⁴⁸ J. Langbehn, Y. Peng, L. Trifunovic, F. von Oppen, and P. W. Brouwer, Reflection-Symmetric Second-Order Topological Insulators and Superconductors, *Phys. Rev. Lett.* **119**, 246401 (2017).
- ⁴⁹ W. A. Benalcazar, B. A. Bernevig, and T. L. Hughes, Quantized electric multipole insulators, *Science* **357**, 61 (2017).
- ⁵⁰ C. Shang, X. N. Zang, W. L. Gao, U. Schwingenschlöggl, and A. Manchon, Second-order topological insulator and fragile topology in topological circuitry simulation, arXiv:2009.09167 (2020).
- ⁵¹ W. A. Benalcazar, B. A. Bernevig, and T. L. Hughes, Electric Multipole Moments, Topological Multipole Moment Pumping, and Chiral Hinge States in Crystalline Insulators, *Phys. Rev. B* **96**, 245115 (2017).
- ⁵² F. Schindler, A. M. Cook, M. G. Vergniory, Z. J. Wang, S. S. P. Parkin, B. A. Bernevig, and T. Neupert, Higher-order topological insulators, *Science Advances.* **4** (2018).
- ⁵³ M. Geier, L. Trifunovic, M. Hoskam, and P. W. Brouwer, Second-order topological insulators and superconductors with an order-two crystalline symmetry, *Phys. Rev. B* **97**, 205135 (2018).
- ⁵⁴ M. Ezawa, Higher-Order Topological Insulators and Semimetals on the Breathing Kagome and Pyrochlore Lattices, *Phys. Rev. Lett.* **120**, 026801 (2018).
- ⁵⁵ C.-H. Hsu, P. Stano, J. Klinovaja, and D. Loss, Majorana Kramers Pairs in Higher-Order Topological Insulators, *Phys. Rev. Lett.* **121**, 196801 (2018).
- ⁵⁶ B. Kang, K. Shiozaki, and G. Y. Cho, Many-body order parameters for multipoles in solids, *Phys. Rev. B* **100**, 245134 (2019).
- ⁵⁷ Y. B. Yang, K. Li, L. M. Duan, and Y. Xu, Higher-order Topological Anderson Insulators, *Phys. Rev. B* **103**, 085408 (2021).
- ⁵⁸ C. A. Li, B. Fu, Z. A. Hu, J. Li, and S. Q. Shen, Topological Phase Transitions in Disordered Electric Quadrupole Insulators, *Phys. Rev. Lett.* **125**, 166801 (2020).
- ⁵⁹ W. A. Wheeler, L. K. Wagner, and T. L. Hughes, Many-body electric multipole operators in extended systems, *Phys. Rev. B* **100**, 245135 (2019).
- ⁶⁰ B. Roy, Antiunitary symmetry protected higher-order topological phases, *Phys. Rev. Research* **1**, 032048 (2019).
- ⁶¹ H. Wu, B. Q. Wang, and J. H. An, Floquet second-order topological insulators in non-Hermitian systems, *Phys. Rev. B* **103**, L041115 (2021).
- ⁶² Z. Zhang, M. R. López, Y. Cheng, X. Liu, J. Christensen, Non-Hermitian Sonic Second-Order Topological Insulator, *Phys. Rev. Lett.* **122**, 195501 (2019).
- ⁶³ E. Edvardsson, F. K. Kunst, E. J. Bergholtz, Non-Hermitian extensions of higher-order topological phases and their biorthogonal bulk-boundary correspondence, *Phys. Rev. B* **99**, 081302 (2019).
- ⁶⁴ D. C. Brody, Biorthogonal quantum mechanics, *J. Phys.A: Math. Theor.* **47**, 035305 (2013).
- ⁶⁵ W. Long, Q. F. Sun, and J. Wang, Disorder-Induced Enhancement of Transport through Graphene p-n Junctions, *Phys. Rev. Lett.* **101**, 166806 (2008).
- ⁶⁶ P. W. Anderson, Absence of Diffusion in Certain Random Lattices, *Phys. Rev.* **109**, 1492-1505 (1958).